

Formation of Sol Gel Dried Droplets of Carbon Doped Titanium Dioxide (TiO₂) at Low Temperature via Electrospraying

S U Halimi¹, S Abd Hashib¹, N F Abu Bakar^{1*}, S N Ismail¹, M Nazli Naim², N Abd Rahman¹ and J Krishnan³

¹Faculty of Chemical Engineering, Universiti Teknologi MARA, MALAYSIA

²Food and Process Department, Faculty of Engineering, Universiti Putra Malaysia (UPM), MALAYSIA

³Department of Chemical Engineering, SSN College of Engineering, Tamilnadu, INDIA

syafiza0358@salam.uitm.edu.my/ fitrah@salam.uitm.edu.my

Abstract. The high band gap energy of TiO₂ and inconsistency in particles size has imposed a significant drawback on TiO₂ applications. Dried droplets of carbon-doped TiO₂ fine particles were produced by using electrospraying technique. The C-doped TiO₂ particles were prepared by hydrolysis of titanium isopropoxide with the addition of carbon precursor followed by electrospraying the suspension in stable Taylor cone-jet mode. Coulomb fission of charged droplets from the electrospraying technique successfully transformed dispersed liquid C-doped TiO₂ particles into solid. The deposited C-doped TiO₂ droplets were collected on aluminium substrates placed at working distances of 10 to 20 cm from the tip of the electrospray needle. The collected C-doped TiO₂ droplets were characterized by using FESEM, UV-Vis, FTIR and XRD. By increasing the working distance, the average droplets size of the deposited C-doped TiO₂ was reduced from ± 163.2 nm to ± 147.56 nm. UV-Vis analysis showed a strong absorption in the visible-light region and about 93 nm red shift of the onset spectrum for C-doped TiO₂. The red shift indicates an increase in photocatalytic efficiency by reducing the TiO₂ band gap energy from 3.0 eV to 2.46 eV and shifting its activity to the visible-light region. FTIR analysis indicated the presence of Ti-C and C-O chemical bonding in the C-doped TiO₂.

1. Introduction

Titanium dioxide (TiO₂) is a promising material that can be used in the degradation of pollutants due to its highly photosensitive, chemically stable, biologically inert and non-toxic in nature. Unfortunately, TiO₂ has a drawback which is high band gap energy (3.2eV) that is activated under ultraviolet light ($\lambda < 387$ nm). The high band gap energy is due to oxygen vacancies and localization of Ti 3d states [1,2]. Other than that, TiO₂ is also thermally unstable which leads to easy phase transformation [3], depending on its synthesis method. To improve TiO₂ properties, methods need to be developed for controlling the droplet size, surface area and morphology, as well as doping with other elements to enhance the photochemical response of TiO₂ towards the visible-light region.

The properties of TiO₂ can be altered by doping, where an impurity is intentionally introduced into TiO₂. There are three opinion regarding the modification mechanism of the doped TiO₂. First is narrowing the TiO₂ bandgap by substituting oxygen in TiO₂ lattice [4], second, introducing an impurity energy level above the valence band [5], and lastly the formation of oxygen vacancy sites as blockers for reoxidation [6]. All three mechanisms lead to improvement of the TiO₂ properties. In this



study, carbon element [7] is chosen as the doping element to produce C-doped TiO₂. Carbon is a promising doping element due to its significant overlapping of electron state between the oxygen near the valence band of TiO₂ [8]. Carbon also has high adsorption capacity, it can be used in both air pollutant degradation and waste water treatment as well as five times more active than nitrogen and other doping element under visible-light irradiation [9]. Methods of producing TiO₂ also have been studied in order to produce C-doped TiO₂ with the desired particle size, morphology and structural characteristic.

Various methods have been used to produce C-doped TiO₂ particles, such as chemical precipitation [10,11,12], sol-gel [13,14] and electrospray drying. In the chemical precipitation method, C-doped TiO₂ suspension needs to be heated rapidly for the hydrolysis process to occur. Precipitates need to be washed and then heated again to produce particles. As a result, the C-doped TiO₂ particles produced from this method are highly aggregated and lead to a wide distribution of particle sizes. In the sol gel method, control of the hydrolysis process is essential in order to obtain a homogenous oxide network. This requires long aging process to form the gel, high calcination temperature to remove organic molecules and grinding process to produce C-doped TiO₂ particles. As a result, the desired anatase phase of C-doped TiO₂ particles was difficult to obtain because of repetition of the heating process and the high calcination temperature. Besides, the produced C-doped TiO₂ also has inconsistent particle sizes due to the grinding process. Therefore, electrospraying technique is introduced in this study as a method to produce fine and uniform C-doped TiO₂ particles without heating at high temperature, aging or grinding process as required in other methods.

Electrospraying or electrohydrodynamic spraying is a method of liquid atomization by electrical forces [15]. It has the ability to produce monodisperse particles, reduce molecular aggregation and operated at ambient condition [16]. The size of the electrospray droplets ranges from hundreds of micrometers down to tens of nanometers. The droplets are highly charged up to a fraction of the Rayleigh limit, which is the maximum charge carried by a droplet. The charge will overcome the liquid surface tension and leads to fission of the droplets. Charged droplets are self-dispersing within the working distance due to the fission process, resulting in the absence of droplets agglomeration [17,18]. Therefore, the electrospraying technique is proposed in this study to produce visible light active C-doped TiO₂ particles.

2. Materials and Methods

2.1 Preparation of C-doped TiO₂ suspension

C-doped TiO₂ suspension was prepared by adding titanium isopropoxide (TTIP) (98%, Sigma-Aldrich Chemie, GmbH) drop-wise as a precursor into 50 mL of deionized water. The mixture was stirred at 500 rpm under room temperature until it turned to cloudy yellow. The cloudy suspension was then dispersed into a mixture of 50 mL ethanol and 10 mL acetic acid (99%, Merck KGaA, Darmstadt Germany). Different concentrations (0.25 M, 0.5 M, 0.75 M and 1.0 M) of acetylacetone (98%, Merck KGaA, Darmstadt Germany) as a dopant precursor were added to the suspension. The suspension was stirred for 1 hour and sonicated (QSonica Sonicators, Q700) at amplitude of 50 kHz for 30 min. The same procedure was used to prepare the un-doped TiO₂ suspension by using TTIP.

2.2 Electrospray deposition of C-doped TiO₂ suspension

Electrospray equipment was set up as shown in Figure 1. The prepared C-doped TiO₂ suspension was loaded into a 25 mL syringe with a needle size of 0.15 mm inside diameter on a syringe pump (SP-1000, Next Advance Inc). The needle tip and counter electrode were connected to an electrostatic generator (G60 EMCO High Voltage). An AC-DC converter (M10-QS305, MCP Lab Electronics) was used to convert alternate current to direct current before connecting it to the electrostatic generator. Positive and negative charge voltage was applied at the needle tip and counter electrode respectively. The flow rate of the C-doped TiO₂ suspension was set at 2.0 mL/h. Voltage was applied in a range of 1.23 to 1.28 kV to maintain the formation of a Taylor cone meniscus at the needle tip. Dispersed C-doped TiO₂ droplets were collected on a flat surface grounded substrate at various working distances (WD) of 10 cm, 15 cm and 20 cm from the counter electrode. The substrate containing deposited droplets were dried in an oven at 60-100 °C for 1 hour.

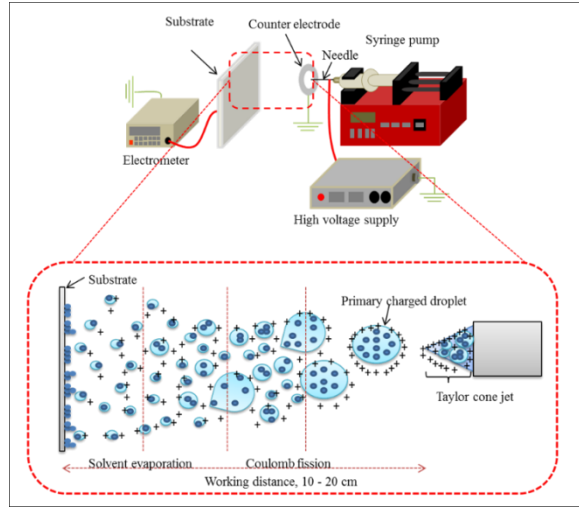


Figure 1. Electro spray setup and mechanism

2.3 Estimation of primary charged droplet size

The primary charged droplet size of C-doped TiO₂ can be estimated by using a scaling law to investigate the droplet fission behaviour of electro spraying, proposed by Hartman et al. [19] Equation (1), Fernandez de la Mora [20] Equation (2) and Ganan-Calvo [21] Equation (3) respectively, as follows:

$$d_d = \left(\frac{\rho \varepsilon_o Q^3}{\gamma K} \right)^{1/6} \quad (1)$$

$$d_d = 1.66 \varepsilon_r^{-1/6} \left(\frac{Q \varepsilon_r \varepsilon_o}{K} \right)^{1/3} \quad (2)$$

$$d_d = 1.2164 \left(\frac{Q \varepsilon_r \varepsilon_o}{K} \right)^{1/3} \quad (3)$$

Where d_d , ρ , ε_o , Q , γ , K and ε_r are the primary droplet size (m), liquid density (kg/m³), electrical permittivity of vacuum (C²/Nm), liquid flow rate (m³/s), surface tension (N/m), conductivity of liquid (S/m) and relative permittivity respectively. Assuming evaporation of droplets occurs without substantial loss of mass by any other mechanism during electro spraying, the theoretical dried droplet size (d_p) can be calculated according to Equation (4).

$$d_p = d_d \theta^{1/3} \quad (4)$$

Where d_p is the theoretical dried droplet size and θ is the volume fraction of material in the solution. The number of fission was determined by dividing the volume of primary charged droplet size over the volume of dried droplets from the diameter of the droplets size of FESEM images. The volume of the droplets is assumed to be spherical. The electro sprayed particles on the substrate were scraped out and characterized using Field Emission Scanning Electron Microscopy (FESEM), UV-Visible Spectroscopy (UV-Vis), Fourier Transform Infrared Spectroscopy (FTIR) and using X-Ray Diffraction (XRD). UV-Visible Spectroscopy (UV-Vis) was used to study the changes in absorption wavelength for both C-doped and un-doped TiO₂ samples. Absorbance data for all samples were recorded at wavelength in a range from 200 nm to 800 nm and presented in a graphical form of absorbance versus wavelength. Fourier Transform Infrared Spectroscopy (FTIR) was used to study changes in functional group for the electro sprayed C-doped TiO₂ samples. The scan spectra were recorded in the range from 500 cm⁻¹ to 4000 cm⁻¹. The crystal phase of the electro sprayed C-doped TiO₂ samples was determined using X-Ray Diffraction (XRD) analysis. The analysis was performed at 40 kV and 150 mA at an angle of 2 θ from 20° to 80°. The scan speed was 1°/min.

3. Results and Discussion

Figure 2 shows the relationship between the zeta potential and particles size in suspensions with various pH. High zeta values were recorded at pH 2 and 13, at 27.98 mV and -45.65 mV respectively. The zeta potential is a term referring to the electrical potential at the boundary of a double layer of particles surface in suspension. Particle suspensions with zeta potential values approximately or closer to ± 30 mV have high degrees of stability [22]. In terms of the particle size in suspensions, at pH 2 and 13, small C-doped TiO₂ particles were obtained with an average size of 249.12 nm and 278.25 nm respectively. Prior to electrospraying, the C-doped TiO₂ suspension was stabilized at pH 2 because this is close to the suspension's initial pH of 3.2. In the acidic condition, the C-doped TiO₂ particles in suspension carried a positive charge as the H⁺ ions surrounded its surface. This condition is similar to the initial condition of the suspension before acid was added to reduce the pH. Thus, only a little acid is required to add into the suspension.

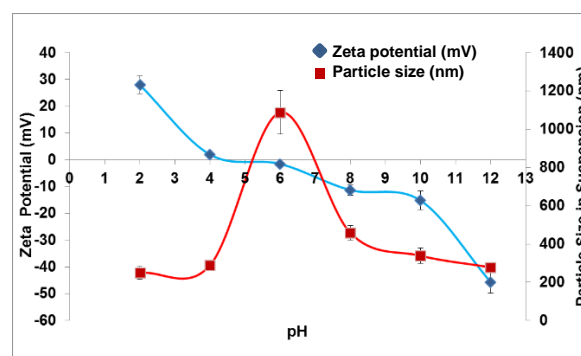


Figure 2. Zeta potential and particles size in suspension versus pH

In this study, the isoelectric point obtained for the C-doped TiO₂ suspension was at pH 4.3. Since no work was found for characterizing the zeta potential of C-doped TiO₂ suspension, the isoelectric point for the C-doped TiO₂ is referred to TiO₂ suspension which has a pH range from 4.0 to 7 [23]. At the isoelectric point, H⁺ and OH⁻ ions are neutralized and there is no charge surrounding the C-doped TiO₂ particles surface. Therefore, C-doped TiO₂ particles tend to flocculate due to the attractive Van der Waals force and later sedimentation occurred. As shown in Figure 2, at pH values near the isoelectric point, the biggest average particle size was recorded at 1088 nm. This is undesirable for C-doped TiO₂ suspension to undergo electrospraying, because it is in an unstable condition. Hence, the C-doped TiO₂ suspension was stabilized at pH 2 prior to electrospraying.

From Figure 3, morphological changes of the C-doped TiO₂ droplets were observed as the working distance (WD) was varied from 10 cm to 20 cm. A wide distribution of dried droplets ranging from 20 to 640 nm with average droplets size of 163.2 nm was observed at 10 cm WD. The droplets size distribution decreased to 20-500 nm and 20-360 nm for WDs of 15 and 20 cm with average droplets size of 162.9 and 147.6 nm respectively. Large C-doped TiO₂ droplets were collected at WDs of 10 cm and 15 cm, which indicated that less fission of primary charged droplets had occurred. The sizes of primary charged droplet, the deposited droplet size and numbers of fission events were estimated and shown in Table 1. Table 2 shows the numbers of fission that occurred during electrospraying increases when the WD increases from 10 cm to 20 cm for each of the scaling law models. From the experimental number of fissions, the number of fission is high for large size of primary charged droplet in agreement with the Fernandez de la Mora model [24], since the conductivity value of C-doped TiO₂ suspension was sufficiently high (i.e. 0.8 S/m) which near to high conductivity condition as in the proposed model. The number of fission from the experiment is in agreement with theoretical number of fission calculated using Fernandez de la Mora model, equation (2). Where the number of fission value at the furthest distance is the closest to the theoretical results derived for the conductivity solution by Fernandez de la Mora [25].

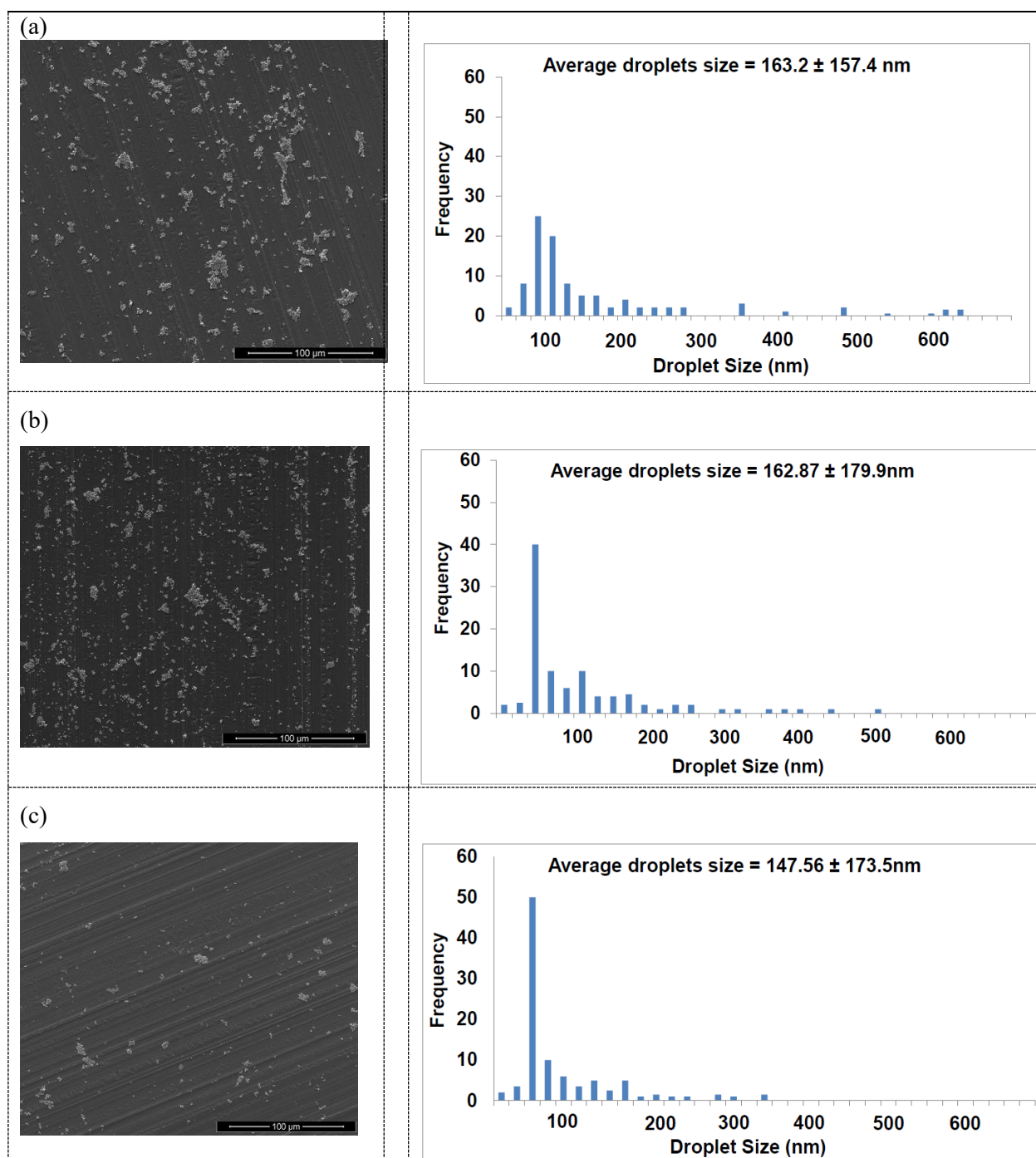


Figure 3. FESEM images and droplets size distribution of deposited 0.5 M C-doped TiO₂ droplets at various WD. (a) 10 cm, (b) 15 cm (c) 20 cm

With increase in WD, the droplets have longer flight and solvent evaporation times, and thus have more time for fission to occur. Hence, this leads to the production of smaller average droplets size. Coulomb fission or explosion of droplets occurs when charged droplets reach the Rayleigh limit. The Rayleigh limit is the maximum amount of charge that a droplet can carry on its surface [26]. When the droplet reaches the Rayleigh limit, it becomes unstable because of the high density of charge on its surface and it breaks up into smaller droplets. The loss of mass during fission is too small to affect the droplet size [27]. The mechanism of Coulomb fission during electrospraying ensure the primary charged droplet underwent fission along the WD before deposited on the substrate [25, 38]. Hence, electrospraying technique could produce a narrow distribution of C-doped TiO₂ droplets with an average droplets size of 147 nm.

Table 1. Estimation of primary and deposited droplets sizes.

Scaling law model	Primary droplet size, d_d (nm)	Theoretical deposited droplets size, d_p from Equation (4) (nm)	Theoretical number of fission
Hartman	2755	642.83	79.02
Fernandez de la Mora	641.46	149.67	79.79
Ganan-Calvo	991.32	231.31	79.03

Table 2. Estimation of experimental number of fission.

Scaling law model	Experimental number of fission, WD = 10 cm	Experimental number of fission, WD = 15 cm	Experimental number of fission, WD = 20 cm
Hartman	4811	4837	6503
Fernandez de la Mora	61	61	82
Ganan-Calvo	224	225	303
Average particle size, $*d_p$ (nm)	163.2	162.9	147.6

* d_p is average deposited droplets size from FESEM image of the respective working distance (WD)

UV-Vis analysis of C-doped samples was performed, and the absorbance spectrum was obtained as shown in Figure 4. The cut-off wavelength for the un-doped TiO_2 sample was ~ 413 nm with calculated band gap energy of 3.0 eV. The absorbance spectrum for un-doped TiO_2 corresponded well with the anatase phase TiO_2 absorbance spectrum from previous work, which has a band gap energy of ~ 3.2 eV [28,29]. For the C-doped TiO_2 samples, the absorption spectrum was red-shifted and the cut-off wavelength was found at 420, 506, 493 and 440 nm for different dopant concentrations of 0.25, 0.5, 0.75 and 1.0 M respectively. An increase in the cut-off wavelength in this study, clearly indicated a decrease in the band gap energy for C-doped TiO_2 samples [30]. The band gap energy can be calculated from the UV-Vis absorbance spectrum and the relation between the band gap energy and cut-off wavelength in the absorption spectra is shown in Equation (5) [31]:

$$\text{Band gap energy } (E_{bg}) = \frac{hc}{\lambda} \quad (5)$$

where h is Plancks constant (6.626×10^{-34} Js), C is the speed of light (3.0×10^8 m/s), λ is the cut-off wavelength of UV-Vis spectra (m) and the conversion factor is 1 eV which is equal to 1.6×10^{-19} J. The calculated band gap energy for doped TiO_2 is shown in Table 3.

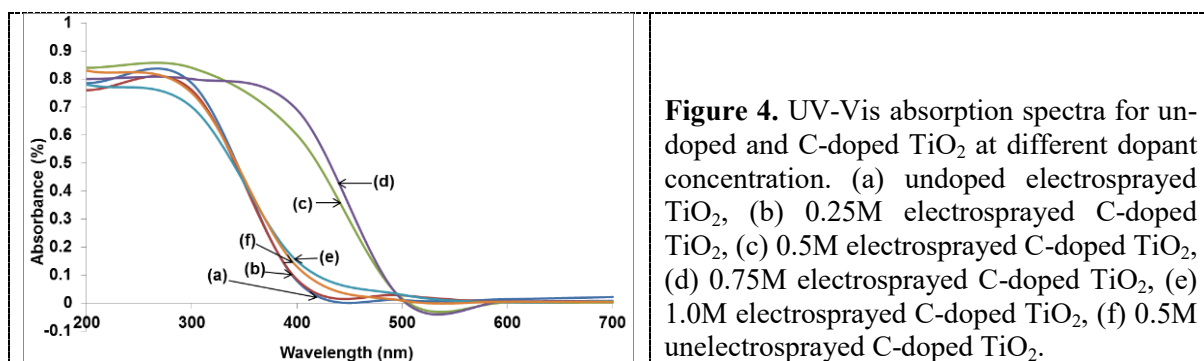


Figure 4. UV-Vis absorption spectra for un-doped and C-doped TiO_2 at different dopant concentration. (a) undoped electrospayed TiO_2 , (b) 0.25M electrospayed C-doped TiO_2 , (c) 0.5M electrospayed C-doped TiO_2 , (d) 0.75M electrospayed C-doped TiO_2 , (e) 1.0M electrospayed C-doped TiO_2 , (f) 0.5M unelectrospayed C-doped TiO_2 .

From Table 3, it is observed that the band gap energy of C-doped TiO_2 is lower than the un-doped TiO_2 . The presence of carbon in C-doped TiO_2 samples creates interface states which result in low band gap energy of TiO_2 [32]. The 0.5 M electrospayed C-doped TiO_2 has the lowest band gap energy compared to other electrospayed C-doped TiO_2 samples, which is 2.46 eV. The lowest band gap energy confirms that 0.5 M electrospayed C-doped TiO_2 has the best properties to be used as photo-catalyst and able to degrade pollutant faster under visible light. The observed variation of the

cut-off wavelength and the pattern of band gap energy depend on the carbon content in the C-doped TiO₂ with varying dopant concentrations. This is because accommodation for carbon substitution in the TiO₂ was limited when the dopant concentration increased. At high dopant concentration which is more than 0.5 M, excess of carbon presents in the samples. The excess carbon in doped TiO₂ might hinder the excitation of electron from valence band to conduction band when the C-doped TiO₂ irradiated under visible light.

Table 3. Band gap energy for un-doped and C-doped TiO₂ sample at different concentration

Sample	Cut off wavelength (m)	E _{bg} (J)	E _{bg} (eV)
Un-doped electrosprayed TiO ₂	4.13×10^{-7}	4.81×10^{-19}	3.00
0.25M electrosprayed C-doped TiO ₂	4.2×10^{-7}	4.73×10^{-19}	2.96
0.5M electrosprayed C-doped TiO ₂	5.06×10^{-7}	3.93×10^{-19}	2.46
0.75M electrosprayed C-doped TiO ₂	4.93×10^{-7}	4.03×10^{-19}	2.52
1.0M electrosprayed C-doped TiO ₂	4.4×10^{-7}	4.52×10^{-19}	2.83
0.5 M un-electrosprayed C-doped TiO ₂	4.3×10^{-7}	4.62×10^{-19}	2.89

Hence, the excess carbon in the 0.75 M and 1.0 M electrosprayed C-doped caused high band gap energy. In summary, carbon in TiO₂ acts as an impurity to form interface states that effectively lower the band gap. As for the 0.5 M unelectrosprayed C-doped TiO₂ sample, the band gap energy obtained is 2.89 eV and the band gap is higher than for the 0.5 M electrosprayed C-doped TiO₂. As discussed earlier, electrosprayed C-doped TiO₂ has a narrow distribution of fined-sized droplets and its high surface area provided more active sites. Hence, the efficiency of electrosprayed C-doped TiO₂ under visible-light irradiation is increased.

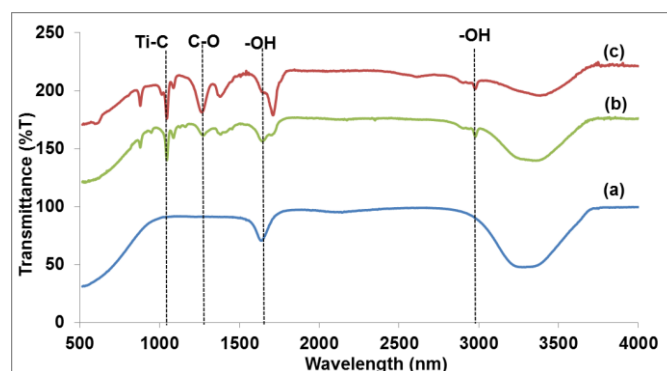


Figure 5. FTIR results for C-doped TiO₂ samples at different dopant concentration. (a) undoped TiO₂, (b) 0.5M unelectrosprayed C-doped TiO₂, (c) 0.5 M electrosprayed C-doped TiO₂

The bonding characteristics of the functional groups in the C-doped TiO₂ samples were identified using FTIR. Figure 5 shows the absorption peaks for un-doped and doped TiO₂ samples. New strong peaks were formed for all the doped TiO₂ samples at around 1044.5, 1263.8, 1650 and 3387 cm⁻¹ [33]. Two peaks at 1044.5 cm⁻¹ and 1263.8 cm⁻¹ represent Ti-C and C-O bonds respectively. The peaks around 1650 cm⁻¹ and 3387 cm⁻¹ represent stretching vibration of OH bonds from surface water molecules and hydroxyl groups in the samples. In the photocatalytic mechanism, hydroxyl groups were trapped in holes that were generated when TiO₂ was irradiated under light. The hydroxyl radicals formed can suppress the recombination of electron-holes [34]. Therefore, the presence of carbon bonding and hydroxyl groups in electrosprayed C-doped TiO₂ shows the improvement in TiO₂ properties.

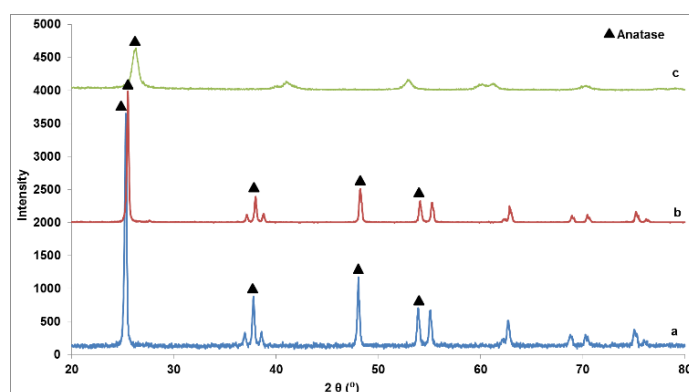


Figure 6: XRD pattern for C-doped TiO₂ samples. (a) undoped electrospun TiO₂, (b) 0.5 M electrospun C-doped TiO₂ (c) 0.5 M un-electrospun C-doped TiO₂

Figure 6 shows the crystalline phase of electrospun C-doped TiO₂. Only anatase phase was present in the C-doped TiO₂ at a diffraction angle of 23°, 37.6°, 48° and 54° [35]. No signals of rutile and brookite phase were detected. The presence of carbon as a doping element in TiO₂ does not induce new crystalline forms other than anatase phase [36]. Acetylacetone used as a source of carbon doping is an organic compound to chelate the titanium atoms and is also responsible for the formation of anatase phase. The intensity of the anatase phase for both 0.5 M electrospun and un-electrospun C-doped TiO₂ was lower than the un-doped TiO₂. This could be due to the low crystalline nature of the carbon element compared to titanium [37]. The reduced intensity of the anatase phase in 0.5 M C-doped TiO₂ is a sign of the presence of carbon in the TiO₂ lattice. However, the peak and intensity of anatase for the un-electrospun 0.5 M C-doped TiO₂ was weak compared to the electrospun sample. In the electrospinning technique, the produced C-doped TiO₂ particles were dried properly, since the mechanism of droplet fission from electrospinning has been proven to facilitate solvent evaporation, so that only dried 0.5 M C-doped TiO₂ particles were collected. For the un-electrospun 0.5 M C-doped TiO₂, the presence of impurities may cause the weak anatase peak formation in the XRD results. Hence, a high drying temperature or calcination process was needed for the un-electrospun 0.5 M C-doped TiO₂ to enhance the formation of the anatase phase.

4. Conclusions

This work demonstrated that the TiO₂ suspension is most stable at pH 2, at which it has a high zeta potential and small particles size in suspension, which is 27.98 mV and 249.12 nm. A stable condition was crucial prior to electrospinning in order to avoid sedimentation of particles during the process. The direct current (DC) voltage applied in the electrospinning method can produce small size droplets with a narrow size distribution and an average droplets size of ±147.56 nm. Increasing the distance from the needle tip to the substrate from 10 cm to 20 cm significantly reduces the deposited droplets size because of Coulomb fission. The fission mechanism was utilized for drying and produces small size droplets with a narrow size distribution. Heating at low temperature was applied for doping the TiO₂ with carbon helps to improve the TiO₂ properties. It lowers the TiO₂ band gap to 2.46 eV and it can be activated under visible-light illumination.

Acknowledgement

The authors would like to express their gratitude to Universiti Teknologi MARA (UiTM) Shah Alam, Malaysia for funding this work. This study was supported by LESTARI Grant 600-IRMI/MYRA 5/3/LESTARI (0143/2016) and Research Entity Initiative (REI) Tier 5, 600-RMI/DANA 5/3 REI (2/2013).

References

- [1] Shen M, Wu Z, Huang H, Yukou D, Zhigang Z, and Ping Y 2006 Carbon-doped anatase TiO₂ obtained from TiC for photocatalysis under visible light irradiation *Journal of Materials Letters* **60** 693-697. doi: 10.1016/j.matlet.2005.09.068
- [2] Cong Y, Zhang J, Chen F, and Anpo M 2007 Synthesis and Characterization of Nitrogen-Doped TiO₂ Nanophotocatalyst with High Visible Light Activity *Journal of Physical Chemistry C*, **111**(19) 6976-6982. doi: 10.1021/jp0685030
- [3] Zhang W, Zou L, and Lianzhou W 2009 Photocatalytic TiO₂/adsorbent nanocomposites prepared via wet chemical impregnation for wastewater treatment A review *Journal of Applied Catalysis A: General* **371** 1-9. doi: 10.1016/j.apcata.2009.09.038
- [4] Asahi R, Morikawa T, Ohwaki T, Aoki K, and Taga Y 2011 Visible-Light Photocatalysis in Nitrogen-Doped Titanium Oxides (Vol. 293). www.sciencemag.org: Toyota Central R&D Laboratories, Nagakute, Aichi 480-1192, Japan
- [5] Irie H, Watanabe Y, and Hashimoto K 2003 Nitrogen-Concentration Dependence on Photocatalytic Activity of TiO₂-xNx Powders *Journal of Physical Chemistry B* **107**(23) 5483-5486. doi: 10.1021/jp030133h
- [6] Aziz A, Cheng C K, Ibrahim S, Matheswaran M, and Saravanan P 2012 Visible light improved, photocatalytic activity of magnetically separable titania nanocomposite *Chemical Engineering Journal* **183**, 349-356.
- [7] Park J H, Kim S, and Allen J B 2006 Novel Carbon-Doped TiO₂ Nanotube Arrays with High Aspect Ratios for Efficient Solar Water Splitting *Nano Letters* **6**(1) 24-28. doi: 10.1021/nl051807y
- [8] Sun Y, Murphy C J, Karla R. Reyes-Gil, Enrique A. Reyes-Garcia, Justin P. Lilliy, and Daniel Raftery 2008 Carbon-doped In₂O₃ films for photochemical hydrogen production *International Journal of Hydrogen Energy* **33** 5967-5974. doi: 10.1016/j.ijhydene.2008.07.100
- [9] Huang Y, W Ho, Shuncheng L, Lizhi Zhang, Guisheng Li, and Jimmy C Y 2008 Effect of Carbon Doping on the Mesoporous Structure of Nanocrystalline Titanium Dioxide and Its Solar-Light-Driven Photocatalytic Degradation of NO_x. *Langmuir* **24** 3510-3516. doi: 10.1021/la703333z
- [10] Chi B, Zhao L, and Tetsuro Jin 2007 One-Step Template-Free Route for Synthesis of Mesoporous N-Doped Titania Spheres *Journal of Physical Chemistry C* **111** 6189-6193. doi: 10.1021/jp067490n
- [11] You X, Chen F, Jinlong Zhang, and Masakazu Anpo 2005 A novel deposition precipitation method for preparation of AG-loaded titanium dioxide *Catalysis Letters* **102**(3-4) 247-250. doi: 10.1007/s10562-005-5863
- [12] Li Y, Hwang D S, Nam Hee L, and Sun-Jae K 2005 Synthesis and characterization of carbon-doped titania as an artificial solar light sensitive photocatalyst *Chemical Physics Letters* **404** 25-29. doi: 10.1016/j.cplett.2005.01.062
- [13] Su C, Hong B Y, and Tseng C M 2004 Sol-gel preparation and photocatalysis of titanium dioxide *Catalysis Today* **96** 119-126. doi: 10.1016/j.cattod.2004.06.132
- [14] Zhu Y, Zhang L, Chong Gao, and Lili Cao 2000 The synthesis of nanosized TiO₂ powder using a sol-gel method with TiCl₄ as a precursor *Journal of Material Science* **35** 4049-4054.
- [15] Jaworek A 2007 Electrospray droplet sources for thin film deposition *Journal of Material Science* **42** 266-297. doi: 10.1007/s10853-006-0842-9
- [16] Jaworek A and Sobczyk A T 2008 Electro spraying route to nanotechnology: An overview *Journal Of Electrostatics* **66** 197-219. doi: 10.1016/j.elstat.2007.10.001
- [17] Hwang D, Lee H, Sung-Yeon J, Seong Mu J, Dongho K, Yongsok S and Dong Young K 2011 Electrospray Preparation of Hierarchically-structured Mesoporous TiO₂ Spheres for Use in Highly Efficient Dye-Sensitized Solar Cells *Applied Materials & Interfaces* **3** 2719-2725. doi: 10.1021/am200517v
- [18] Jayasinghe S N 2008 Electrospray Self-assembly: An emerging jet-based route for directly forming nanoscaled structures *Journal of Physica E* **40** 2911-2915. doi: 10.1016/j.physe.2008.02.005

- [19] Yuteri C U, Hartman R P A and Marijnissen J C M 2010 Producing Pharmaceutical Particles via Electro spraying with an Emphasis on Nano and Nano Structured *KONA Powder and Particle Journal* **28** 91-115.
- [20] Kulkarni P, Baron P A and Klaus Willeke. 2011 Scaling Laws, Required Liquid Physical Properties, and Operating Domain *Aerosol Measurement: Principle, Technique and Applications* (Vol. Third Edition): John Wiley & Sons.
- [21] Ganan-Calvo A M 1998 The Surface Charge In Electro spraying: Its Nature and Its Universal Scaling Laws *Journal Of Aerosol Science* **30**(7) 863-872. doi: 0021-8502/99/\$
- [22] Greenwood R 2003 Review of the measurement of zeta potentials in concentrated aqueous suspension using electroacoustics *Advances in Colloid and Interface Science* **106** 55-81. doi: 10.1016/S0001-8686(03)00105-2
- [23] Schneider C, Hanisch M, Bastian Wedel, Arben Jusufi and Matthias Ballauff 2011 Experimental study of electrostatically stabilized colloidal particles: Colloidal stability and charge reversal *Journal of Colloid and Interface Science* **358** 62-67. doi: 10.1016/j.jcis.2011.02.039
- [24] Rohner T C, Lion N and Hubert H. Girault 2004 Electrochemical and theoretical aspects of electrospray ionisation *Physical Chemistry* **6** 3056-3068.
- [25] Zolkepalı N K, Noor Fitrah Abu Bakar, M. Nazli Naim, Nornizar Anuar, Nurul Fadhilah Kamalul Aripin, Mohd Rushdi Abu Bakar, I. Wuled Lenggoro, Hidehiro Kamiya 2016 Formation of Fine and Encapsulated Mefenamic Acid Form I Particles for Dissolution Improvement via Electrospray Method *Particulates and Science Technology*. doi: 10.1080/02726351.2016.1246496
- [26] Gu W, Heil P E, Hyungsoo C and Kyekyoon K 2007 Comprehensive model for fine Coulomb fission of liquid droplets charged to Rayleigh limit *Applied Physics Letters* **91**(064104). doi: 10.1063/1.2767774
- [27] Saalah S, M. Nazli Naim, Mohd. Noriznan Mokhtar, Noor Fitrah Abu Bakar, Masao Gen, and I. Wuled Lenggoro 2014 Transformation of cyclodextrin glucanotransferase (CGTase) from aqueous suspension to fine solid particles via electrospraying *Journal of Enzyme and Microbial Technology* **64-65** 52-59. doi: 10.1016/j.enzmitec.2014.06.002
- [28] Scanlon D O, Dunnill C W, John Buckeridge, Stephen A. Shevlin, Andrew J. Longsdail, Scott M. Woodley, C. Richard A. Catlow, Michael J. Powell, Robert G. Palgrave, Ivan P. Parkin, Graeme W. Watson, Thomas W. Keal, Paul Sherwood, Aron Walsh, and Alexey A. Sokol 2013 Band alignment of rutile and anatase TiO₂ *Nature Materials* **12** 798-801. doi: 10.1038/NMAT3697
- [29] Reddy K M, Manorama S V and A Ramachandra Reddy 2002 Bandgap studies on anatase titanium dioxide nanoparticles *Materials Chemistry and Physics* **78**, 239-245.
- [30] Wang G, Xu L, Jun Zhang, Tingting Yin and Deyan Han 2011 Enhance Photocatalytic Activity of TiO₂ Powders (P25) via Calcination Treatment. Hubei Normal University, Huangshi, Hubei, China. International Journal of Photoenergy
- [31] PerkinElmer 2009 UV/Vis/NIR Spectrometer *Simple Method of Measuring the Band Gap Energy Value of TiO₂ in the Powder Form using a UV/Vis/NIR Spectrometer*. Shelton, CT USA: PerkinElmer.
- [32] Lin Y T, Weng C H, Yu-Hao Lin, Ching-Chang Shiesh and Fang-Ying Chen 2012 Effect of C content and calcination temperature on the photocatalytic activity of C-doped TiO₂ catalyst *Journal of Separation and Purification Technology* **116** 114-123. doi: 10.1016/j.seppur.2013.05.018
- [33] Khalil K M S, Baird T, Mohamed I. Zaki, Ahmed A. El-Samahy and Aida M. Awad 1998 Synthesis and characterization of catalytic titanias via hydrolysis of titanium (IV) isopropoxide *Journal of Colloids and Surfaces A: Physicochemical and Engineering Aspects* **132** 31-44.
- [34] Dong F, Wang H and Zhongbiao Wu 2009 One-Step "Green" Synthetic Approach for Mesoporous C-Doped Titanium Dioxide with Efficient Visible Light Photocatalytic Activity *Journal of Physical Chemistry C* **113** 16717-16723. doi: 10.1021/jp9049654
- [35] Wang H, Wu Z and Yue Liu 2009 A Simple Two-Step Template Approach for Preparing Carbon-Doped Mesoporous TiO₂ Hollow Microspheres *Journal of Physical Chemistry C* **113** 13317-13324. doi: 10.1021/jp9147693

- [36] Anson-Casaos A, Tacchini I, Andrea Unzue and M. Teresa Martinez 2013 Combined modification of a TiO₂ photocatalyst with two different carbon forms *Applied Surface Science* **270** 675-684.
- [37] Yue L, Hai-qiang W and Wu Zhong-biao 2007 Characterization of metal doped-titanium dioxide and behaviours on photocatalytic oxidation of nitrogen oxides *Journal of Environmental Sciences* **19** 1505-1509.
- [38] Naim M N, Abu Bakar N F, Iijima M, Kamiya H, and Lenggoro I W, Electrostatic Deposition of Aerosol Particles Generated from an Aqueous Nanopowder Suspension on a Chemically Treated Substrate *Japanese Journal of Applied Physics* **49** (2010) 06GH17 1-6